

## Imprint of Gravitational Waves on the Cosmic Microwave Background

Robert Crittenden,<sup>1</sup> J. Richard Bond,<sup>2</sup> Richard L. Davis,<sup>1</sup> George Efstathiou,<sup>3</sup> and Paul J. Steinhardt<sup>1</sup>

<sup>1</sup>*Department of Physics, University of Pennsylvania, Philadelphia, Pennsylvania 19104*

<sup>2</sup>*Canadian Institute for Theoretical Astrophysics, University of Toronto, Toronto, Ontario, Canada M5S 1A7*

<sup>3</sup>*Department of Astrophysics, Oxford University, Oxford, England OX1 3RH*

(Received 25 March 1993)

Long-wavelength gravitational waves can induce significant temperature anisotropy in the cosmic microwave background. Distinguishing this from anisotropy induced by energy density fluctuations is critical for testing inflationary cosmology and theories of large-scale structure formation. We describe full radiative transport calculations of the two contributions and show that they differ dramatically at angular scales below a few degrees. We show how anisotropy experiments probing large- and small-angular scales can combine to distinguish the imprint due to gravitational waves.

PACS numbers: 98.80.Cq, 04.30.+x, 98.70.Vc

The cosmic microwave background (CMB) temperature anisotropy may be induced by energy density fluctuations *and* by gravitational waves [1], corresponding to scalar and tensor metric perturbations, respectively. Although anisotropy measurements probing angular scales above a few degrees [e.g., those from the Cosmic Background Explorer (COBE) [2]] cannot discriminate scalar from tensor [3], we show in this Letter that the two contributions can be separated when data from smaller angle experiments are used as well.

Resolving the two contributions relies upon detailed theoretical predictions for the form of the multipole components,  $a_{\ell m}^{(S)}$  and  $a_{\ell m}^{(T)}$ , of the relative temperature pattern on the sky,  $\Delta T/T(\theta, \phi)$ . For inflationary models, each multipole for the two modes is predicted to be statistically independent and Gaussian distributed, fully specified by angular power spectra,  $C_{\ell}^{(S)} = \langle |a_{\ell m}^{(S)}|^2 \rangle$  and  $C_{\ell}^{(T)} = \langle |a_{\ell m}^{(T)}|^2 \rangle$ . Although  $C_{\ell}^{(S)}$  has been calculated before [4],  $C_{\ell}^{(T)}$  was previously known only for low multipoles,  $\ell \lesssim 30$ , relevant for angles above a few degrees [1,3,5]. For these  $\ell$ 's, the dominant spatial wavelengths contributing to  $C_{\ell}^{(T)}$  and  $C_{\ell}^{(S)}$  were outside the horizon at photon decoupling, and both scalar and tensor modes induce similar redshifts and blueshifts in the CMB [1,3,5]. For example, COBE's differential microwave radiometer (DMR) is unable to distinguish the two contributions due to cosmic variance (from the theory signal) and experimental noise, although their sum can be determined from one year of DMR data to within 30% [see Fig. 2(a) below], improving to about 15% with four full years of data.

In this Letter, we compute  $C_{\ell}^{(T)}$  to much higher multipoles, and show that the predicted  $C_{\ell}^{(T)}$  becomes highly suppressed relative to  $C_{\ell}^{(S)}$  at large  $\ell$ . The dominant wavelengths for  $\ell \gtrsim 30$  were inside the horizon at decoupling. Inside the horizon, scalar-mode anisotropies are enhanced by the gravitational instability of density perturbations and by Thomson scattering from moving electrons, whereas gravitational waves disperse as freely propagating, massless excitations and redshift away.

Taking advantage of this difference, we find that combining experiments at small- and large-angular scales can determine the scalar and tensor components. Current CMB anisotropy data at small scales are not yet good enough to do so, especially since some of the signals observed may be galactic rather than cosmic in origin, but the statistical errors of these and other near-future experiments are small enough to allow separation at about the two sigma level, as we show here.

Separating tensor from scalar is essential for theories of cosmic structure formation since it is from  $C_{\ell}^{(S)}$  that we can infer the primordial density fluctuations. It also provides a critical test for inflationary cosmology [3,5,6]. All inflation models produce a postinflation spectrum of scalar and tensor metric fluctuations with some tilt away from strict scale-invariant form (scalar spectral index  $n_s = 1$ , tensor index  $n_t = 0$ ). In fact, inflation predicts a relation between the gravitational wave content of the CMB anisotropy and the tilt [3,5,6]:

$$C_2^{(T)}/C_2^{(S)} \approx -7n_t \approx 7[1 - n_s + \delta]. \quad (1)$$

$C_2^{(T)}$  and  $C_2^{(S)}$  are the  $\ell = 2$  (quadrupole) components of the power spectrum and  $\delta \equiv (2V'/3H^2)'$  where  $V$  and  $H$  are the inflaton potential and the Hubble constant, respectively, evaluated sixty  $e$ -folds before the end of inflation (prime denotes derivative with respect to the inflaton field). Both  $\delta$  and corrections to Eq. (1) are negligibly small (hence,  $n_t \approx 1 - n_s$ ) for generic models of inflation, including extended, natural, chaotic, power-law, or new inflation. [The only known exceptions are cases where  $\delta$  is made non-negligible by artificially fine tuning  $V$  such that the inflaton lies near an inflection point ( $V' = 0$ ;  $V'' \neq 0$ ) or along a linear ramp ( $V' \neq 0$ ;  $V'' = 0$ ) just sixty  $e$ -folds before the end of inflation. For this study, we will ignore these exceptional cases.] Confirmation of Eq. (1) would be new support for inflation providing detailed information about the first instants of the Universe.

For a given sum of  $C_{\ell}^{(T)}$  and  $C_{\ell}^{(S)}$  fixed by large-angular scale measurements, a larger tensor component reduces the small-angle anisotropy. Several other factors can have

a qualitatively similar effect (e.g., increased tilt,  $1 - n_s$ ; decreased baryon density,  $\Omega_B$ ; and a nonstandard recombination history), but there are quantitative differences which we now describe.

To compute  $C_\ell^{(T)}$ , we evolve the distribution function,  $\mathbf{f}(\mathbf{x}, \mathbf{q}, t)$ , for photons at position  $\mathbf{x}$  at time  $t$  with momentum  $\mathbf{q}$ , using first-order perturbation theory of the general relativistic Boltzmann equation for radiative transfer [4], with a Thomson scattering source term. Photon polarization is included by making  $\mathbf{f}$  a four-dimensional vector with components related to the Stokes parameters ( $f_s$  with  $s = t, p, u, v$  correspond to the usual  $I, Q, U, V$  Stokes notation) and applying Chandrasekhar's development of the scattering source term for Rayleigh (and thus Thomson) scattering in a plane parallel atmosphere [7]. In the scalar case, only  $f_t$  and the "polarization"  $f_p$  are needed, so two transfer equations are required [4]. In the tensor case  $f_u$  also does not vanish, but it is related to  $f_p$ , so again only two perturbed transfer equations turn out to be required. To describe these equations, we introduce the relative perturbed distribution functions [4]  $\Delta_s^{(T)} = 4\delta f_s / (T_0 \partial \bar{f} / \partial T_0)$ , where  $T_0$  is the CMB temperature and  $\bar{f}$  is the unperturbed Planck distribution.

To evolve the coupled equations, both  $\Delta_s^{(T)}$  and the metric are expanded in plane waves. In the frame in which the wave vector  $\mathbf{k}$  is along the  $z$  axis, the gravitational wave degrees of freedom in the metric are the transverse traceless modes  $h_+ = h_{11} = -h_{22}$  and  $h_\times = h_{12} = h_{21}$ , which obey an Einstein equation, the wave equation for free massless particles:  $\ddot{h}_\epsilon + 2\frac{\dot{a}}{a}\dot{h}_\epsilon + k^2 h_\epsilon = 0$ ,  $\epsilon = +, \times$ . Here the dot denotes derivative *wrt* conformal time,  $\tau = \int dt/a(t)$  where  $a$  is the expansion factor,

solved by evolving the Friedmann equation.

The radiative transfer equations for the two gravity wave polarizations separate, having an overall factor of  $\cos(2\phi)$  for  $\epsilon = +$  and of  $\sin(2\phi)$  for  $\epsilon = \times$ , where  $(\theta, \phi)$  are the polar angles, which we remove by introducing new variables, following Polnarev [8],

$$\begin{aligned}\Delta_t^{(T)} &= \tilde{\Delta}_{t+}^{(T)}(1 - \mu^2) \cos 2\phi + \tilde{\Delta}_{t\times}^{(T)}(1 - \mu^2) \sin 2\phi, \\ \Delta_p^{(T)} &= \tilde{\Delta}_{p+}^{(T)}(1 + \mu^2) \cos 2\phi + \tilde{\Delta}_{p\times}^{(T)}(1 + \mu^2) \sin 2\phi, \\ \Delta_u^{(T)} &= -\tilde{\Delta}_{u+}^{(T)}2\mu \sin 2\phi + \tilde{\Delta}_{u\times}^{(T)}2\mu \cos 2\phi,\end{aligned}\quad (2)$$

where  $\mu = \hat{\mathbf{k}} \cdot \hat{\mathbf{q}}$  and  $q$  is the comoving photon momentum. The combination  $\tilde{\Delta}_{p\epsilon}^{(T)} + \tilde{\Delta}_{u\epsilon}^{(T)}$  is unexcited by gravity waves, as is  $\Delta_v^{(T)}$ , so the four Stokes radiative transfer equations reduce to two:

$$\begin{aligned}\tilde{\Delta}_{t\epsilon}^{(T)} &= -ik\mu\tilde{\Delta}_{t\epsilon}^{(T)} - \dot{h}_\epsilon - a\sigma_T n_e \tilde{\Delta}_{t\epsilon}^{(T)} + a\sigma_T n_e \Psi_\epsilon, \\ \tilde{\Delta}_{p\epsilon}^{(T)} &= -ik\mu\tilde{\Delta}_{p\epsilon}^{(T)} - a\sigma_T n_e \tilde{\Delta}_{p\epsilon}^{(T)} - a\sigma_T n_e \Psi_\epsilon, \\ \Psi_\epsilon &\equiv \left[ \frac{1}{10}\tilde{\Delta}_{t\epsilon,0}^{(T)} - \frac{1}{7}\tilde{\Delta}_{t\epsilon,2}^{(T)} + \frac{3}{70}\tilde{\Delta}_{t\epsilon,4}^{(T)} \right. \\ &\quad \left. - \frac{3}{5}\tilde{\Delta}_{p\epsilon,0}^{(T)} - \frac{6}{7}\tilde{\Delta}_{p\epsilon,2}^{(T)} - \frac{3}{70}\tilde{\Delta}_{p\epsilon,4}^{(T)} \right].\end{aligned}\quad (3)$$

Here  $\sigma_T$  is the Thomson scattering cross section, and  $n_e$ , the free electron density, is evolved using a careful treatment of the recombination atomic physics.

As in the scalar case [4], we solve these equations by expanding in Legendre polynomials, e.g.,  $\tilde{\Delta}_{t\epsilon} = \sum_\ell (2\ell + 1)\tilde{\Delta}_{t\epsilon,\ell} P_\ell(\mu)$ , converting (3) to a hierarchy of coupled equations. Our solutions,  $\tilde{\Delta}_{t\epsilon,\ell}(k, \tau)$  and  $\tilde{\Delta}_{p\epsilon,\ell}(k, \tau)$ , can be combined into the power spectrum by summing over  $\mathbf{k}$  and polarizations

$$C_\ell^{(T)} = \frac{\pi}{2} \sum_{\mathbf{k}} (\ell - 1)\ell(\ell + 1)(\ell + 2) \left\langle \left| \frac{\tilde{\Delta}_{tG,\ell-2}}{(2\ell - 1)(2\ell + 1)} - 2 \frac{\tilde{\Delta}_{tG,\ell}}{(2\ell - 1)(2\ell + 3)} + \frac{\tilde{\Delta}_{tG,\ell+2}}{(2\ell + 1)(2\ell + 3)} \right|^2 \right\rangle, \quad (4)$$

where  $\tilde{\Delta}_{tG,\ell} \equiv (\tilde{\Delta}_{t+,\ell} - i\tilde{\Delta}_{t\times,\ell})/\sqrt{2}$ . A similar expression applies for the polarization power spectrum [9]. A useful check is to assume recombination is sudden at  $\tau = \tau_r$ . The free-streaming solution from  $\tau_r$  to the present  $\tau_0$  is then  $\tilde{\Delta}_{t\epsilon,\ell} = (-i)^\ell \int_{\tau_r}^{\tau_0} d\tau j_\ell[k(\tau_0 - \tau)]\dot{h}_\epsilon(\tau)$ . Substitution into Eq. (4) gives the Abbott and Wise [1] formula for  $C_\ell^{(T)}$ , with which our numerical results agree for low  $\ell$ .

In this paper, we discuss results for standard cold dark matter (CDM) models with normal recombination, although it is straightforward to adapt the numerical codes to other cosmological models (e.g., mixed hot and cold dark matter). We let  $n_s$ , the ratio of tensor-to-scalar quadrupole anisotropy, the baryon density  $\Omega_B$ , and the Hubble parameter [10]  $h$  vary freely.

Figure 1 shows a CDM model with  $\Omega_B = 0.05$ ,  $h = 0.5$ , and  $n_s = 0.85$ , which accounts for the slight downward tilt in  $C_\ell^{(S)}$  at small  $\ell$ . [We plot  $\ell(\ell + 1)C_\ell$ , since it is flat for scale-invariant ( $n_s = 1$ )  $C_\ell^{(S)}$  at small  $\ell$ .] The sharp increase in  $C_\ell^{(S)}$  for  $\ell \gtrsim 50$  followed by increasingly

damped oscillations is due to adiabatic compression of photons and Doppler shifts during decoupling [4]. In contrast, the tensor moments drop sharply; then the curve settles to a tilted spectrum similar to the scalar case for  $5 \lesssim \ell \lesssim 50$ . At  $\ell \gtrsim 50$ , the tensor drops sharply just as the scalar rises. We have set  $C_2^{(T)}/C_2^{(S)} \approx 1$ , the inflation prediction of Eq. (1) for a tilt of  $n_s = 0.85$ . We also illustrate how a scalar-only spectrum with low  $\Omega_B$  (e.g., the dashed curve) partially mimics the scalar-plus-tensor shape for  $\Omega_B = 0.05$  (assuming a larger  $C_2^{(S)}$ ). Clearly, precise measurements are required to separately determine  $C_2^{(T)}/C_2^{(S)}$  and  $\Omega_B$ .

The filter functions are shown for various experiments in Fig. 1(b). The theoretical prediction for the rms fluctuations is found by multiplying  $C_\ell/4\pi$  by the filter and summing over  $\ell, m$ . From Fig. 1, we see that large-angle experiments (e.g., DMR [2], MIT [11], and Tenerife [12]) are equally sensitive to tensor and scalar modes, smaller-

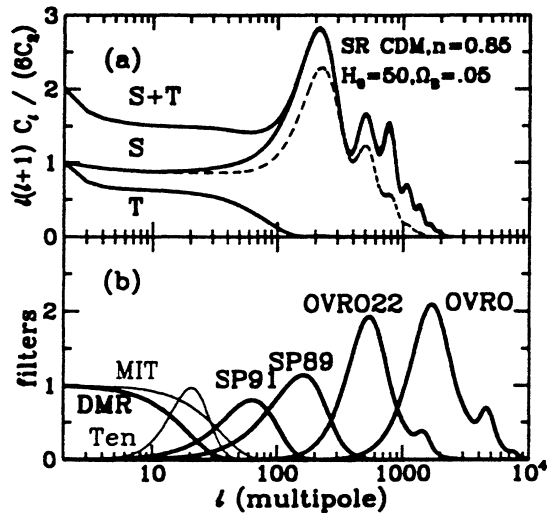


FIG. 1. (a) Angular power spectra for the tilted standard CDM model shown for tensor, scalar, and the sum. The light dashed line is an  $\Omega_B = 0.01$  model. (b) shows the filters for the experiments used in this paper as examples (heavy lines). The light lines are other representative experiments.

angle experiments (e.g., SP89 [13] and OVRO [14]) are sensitive mostly to scalar, while the intermediate SP91 [15,16] can measure some tensor, although predominantly scalar.

A quantitative experimental fit to cosmological parameters is obtained by constructing likelihood functions  $\mathcal{L}_e(C_2^{(S)}, C_2^{(T)}, n_s, \Omega_B, h)$  for each experiment,  $e$ , assuming Gaussian statistics [17]. Assuming the experiments are statistically independent (because they cover unrelated regions of the sky or very different angular wave bands), we combine the  $\mathcal{L}_e$ 's to get the full likelihood,  $\mathcal{L} = \prod_e \mathcal{L}_e$ , as shown in Fig. 2. For all but DMR,  $\mathcal{L}_e$  is calculated using Bayesian techniques [17] which take into account the removal of any linear combinations of the data such as gradients or averages by marginalizing over the coefficients, assuming uniform prior probability distribution in these coefficients. For SP91, the method was extended to treat simultaneously the four frequency channels. For DMR, we used the Smoot *et al.* "90  $A + B \times 53 A + B$ " (quadrupole-subtracted) correlation function [2] with a Gaussian approximation for the likelihood [18]. A more complete analysis will only be possible once the DMR data are released. In Fig. 2, we have taken  $\Omega_B = 0.05(2h)^{-2}$ , consistent with nucleosynthesis limits [19], and  $h = 0.5$ .

Figure 2(a) displays the DMR likelihood contours in the  $C_2^{(S)} - C_2^{(T)}$  plane for fixed  $n_s$  (0.85), demonstrating that DMR can measure  $C_2^{(S)} + C_2^{(T)}$ , but cannot discriminate scalar and tensor. A preferred tensor-scalar ratio does arise in Fig. 2(b) as soon as we incorporate small-angle data. Figure 2(b) combines the DMR data and the 4-frequency-channel data from a 9 point strip [15] and

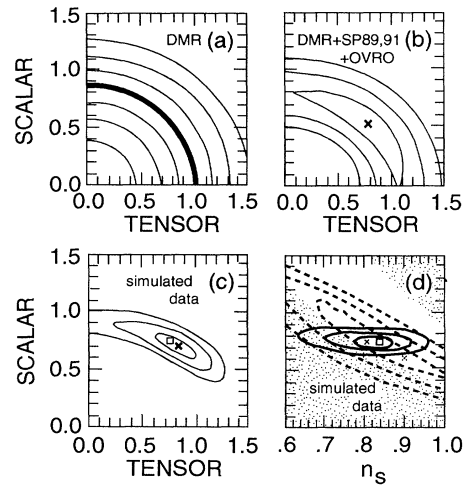


FIG. 2. Likelihood contour maps for scalar ( $[C_2^{(S)}]^{1/2}/10^{-5}$ ) vs tensor ( $[C_2^{(T)}]^{1/2}/10^{-5}$ ) amplitudes are shown in (a), (b), and (c) for the standard CDM model with fixed  $n_s = 0.85$  tilt. The light curves are 1, 2, and 3 sigma lines, the heavy curve or  $\times$  gives the maximum likelihood. (a) DMR only. (b) DMR plus the 9 and 13 point SP91 data, along with SP89 plus OVRO. (c) shows the maps with simulated large- and small-angle data consisting of DMR (with 4 year error bars), six 13 point SP91 strips, six 9 point SP89 strips, and one OVRO22 strip. The mean CDM signal input into the simulated data is denoted by the square. (d) shows 1, 2, and 3 sigma likelihood contours for the simulated data in  $[C_2^{(S)}]^{1/2} - n_s$  space, constrained to the  $C_2^{(T)}/C_2^{(S)}$  trajectory defined by Eq. (1) (solid) and the unconstrained maximum likelihood trajectory (dashed). Shading indicates the range for which CDM models are not dynamically viable.

a 13 point strip [16] in the SP91 experiment, as well as SP89 [13] and OVRO [14] data (which give weak upper limits but no detections). For simplicity, errors in the different frequency channels and between the two strips are treated as uncorrelated. There appear to be detections, but the signal may be contaminated by unknown sources.

Figure 2(b) is tantalizing but inconclusive evidence for a gravitational wave contribution. Future refinement can be anticipated by using simulated data sets, constructed by taking single realizations of theoretical signals and adding experimental noise associated with statistical errors (but no systematic errors). In Figs. 2(c) and 2(d), the input signal is for a standard CDM model with  $n_s = 0.85$  and equal  $C_2^{(T)}$  and  $C_2^{(S)}$  ( $[7.5 \times 10^{-6}]^2$ ). We then simulate a suite of plausible forthcoming experiments: DMR with 4-year error bars; six 13 point strips from an SP91 configuration (18–27  $\mu\text{K}$  error bars for each of the four frequency channels); six 9 point strips from an SP89 [13] configuration; and an OVRO22 configuration (7' beam, 22' double-difference throw, with 25  $\mu\text{K}$  error bars). Reduced ( $\approx 15 \mu\text{K}$ ) error bars were taken for SP89 to represent ongoing or planned experiments with

beams  $\sim 0.5^\circ$  which, with multifrequency observations, can achieve these sensitivities [20].

Figure 2(d) shows two projections onto the  $C_2^{(S)}$ - $n_s$  plane. The heavy contours are the likelihood if  $C_2^{(T)}/C_2^{(S)}$  is restricted to the trajectories predicted by inflation, Eq. (1). The maximum lies within 10% of the input signal. In contrast, the light curves show the contours when the (unrestricted) maximum likelihood value for the given  $C_2^{(S)}$  and  $n_s$  is taken. The extended 1 sigma band along  $C_2^{(T)}/C_2^{(S)} \approx [2 - 5.2(1 - n_s)]^2$  indicates an inability to distinguish large tilt from large tensor component for these sensitivities. The band runs across the inflation prediction (heavy lines), intersecting in a narrow range about  $n_s \approx 0.83$ , very close to the input value.

We conclude that current and near-future anisotropy experiments are unable by themselves to definitively test inflation [Eq. (1)] or determine the gravitational wave contribution to the CMB. For the short term, conclusions can only be drawn by adding extra assumptions and/or other data. For example, we have shown in Figs. 2(c) and 2(d) that, if Eq. (1) is assumed,  $n_s$  and the gravitational wave imprint can be determined to within 2 sigma. Alternatively, other cosmological constraints can be invoked. For example, a variety of arguments imply that the rms amplitude of the density fluctuations on scales of  $8h^{-1}\text{Mpc}$  ( $\sigma_8$ ), which is used to measure the amount of nonlinear dynamics in large-scale structure calculations, cannot lie outside of the range 0.45 and 1 for CDM ( $\Omega = 1$ ) models [6,21]; this translates to the shaded region in Fig. 2(d). If one assumes a model of galaxy clustering with linear biasing, a tilt  $n_s \lesssim 0.65$  is required for standard CDM models to reproduce the galaxy correlation function [6] (which would exclude our input model). This restriction may be relaxed with less simplistic CDM models of galaxy formation, and in cosmologies with more power in the density fluctuations than CDM has on large scales [21].

The long-term future is brighter. Extensive mapping of the microwave sky on small- and intermediate-angular scales can lead to highly accurate determinations of the spectrum; e.g., we find that the limiting cosmic variance uncertainty in  $\Delta T/T$  is only a few percent for SP89 and SP91 configurations. Even at large angles where cosmic variance is higher, we find that 5% accuracy should be achievable. Hence, given optimal experimental designs, there should be sufficient resolution for a fully independent test for inflation, theories of large-scale structure, and the imprint of gravitational waves.

We thank P. Lubin and M. Turner for useful conversations. This research was supported by the DOE at Penn (DOE-EY-76-C-02-3071), NSERC at Toronto, the SERC at Oxford, and the Canadian Institute for Advanced Re-

search.

- 
- [1] L.F. Abbott and M. Wise, Nucl. Phys. **B244**, 541 (1984); A.I. Starobinsky, Pis'ma Astron. Zh. **11**, 323 (1985) [Sov. Astron. Lett. **11**, 133 (1985)].
  - [2] G.F. Smoot *et al.*, Astrophys. J. Lett. **396**, L1 (1992).
  - [3] R.L. Davis, H.M. Hodges, G.F. Smoot, P.J. Steinhardt, and M.S. Turner, Phys. Rev. Lett. **69**, 1856 (1992).
  - [4] J.R. Bond and G. Efstathiou, Astrophys. J. **285**, L45 (1984); Mon. Not. R. Astron. Soc. **226**, 655-687 (1987); J.R. Bond, in *The Early Universe*, edited by W. Unruh and G. Semenoff (Reidel, Dordrecht, 1988); G. Efstathiou, in *Physics of the Early Universe*, edited by A. Heavens, A. Davies, and J. Peacock (Scottish Universities Summer School Publications, Edinburgh, 1990).
  - [5] F. Lucchin, S. Matarrese, and S. Mollerach, Astrophys. J. Lett. **401**, 49 (1992); D. Salopek, Phys. Rev. Lett. **69**, 3602 (1992); A. Liddle and D. Lyth, Phys. Lett. B **291**, 391 (1992); V. Sahni and T. Souradeep, Mod. Phys. Lett. A **7**, 3541 (1992); J.E. Lidsey and P. Coles, Mon. Not. R. Astron. Soc. **258**, 57P (1992).
  - [6] F.C. Adams, J.R. Bond, K. Freese, J.A. Frieman, and A.V. Olinto, Phys. Rev. D **47**, 426 (1993).
  - [7] S. Chandrasekhar, *Radiation Transfer* (Dover, New York, 1960), pp. 1-53.
  - [8] A.G. Polnarev, Astron. Zh. **29**, 1041 (1985) [Sov. Astron. **29**, 607 (1985)].
  - [9] We find the polarization induced by the tensor mode is negligibly small ( $\ll 1\%$ ), whereas models with early reionization have significant polarization, an added discriminant that we will not explore here.
  - [10]  $H_0 = 100h \text{ km s}^{-1} \text{ Mpc}^{-1}$ .
  - [11] K. Ganga *et al.* (to be published).
  - [12] A. Lasenby *et al.* (to be published).
  - [13] P. Meinhold and P. Lubin, Astrophys. J. Lett. **370**, 11 (1991).
  - [14] A.C.S. Readhead *et al.* Astrophys. J. **346**, 556 (1989).
  - [15] T. Gaier, J. Schuster, J. Gunderson, T. Koch, M. Seiffert, P. Meinhold, and P. Lubin, Astrophys. J. Lett. **398**, L1 (1992).
  - [16] J. Schuster *et al.* (to be published).
  - [17] J.R. Bond, G. Efstathiou, P.M. Lubin, and P. Meinhold, Phys. Rev. Lett. **66**, 2179 (1991).
  - [18] The Gaussian variance for the likelihood adds to the observational errors [2] an all-sky cosmic variance and a (small) signal-noise interference variance computed assuming a uniform pixel noise which best fits the DMR error bars.
  - [19] T.P. Walker, G. Steigman, D.N. Schramm, K.A. Olive, and H.S. Kang, Astrophys. J. **376**, 51 (1991).
  - [20] E.g., P. Meinhold *et al.* (to be published); J. Gunderson *et al.* (to be published).
  - [21] G. Efstathiou, J.R. Bond, and S.D.M. White, Mon. Not. R. Astron. Soc. **258**, 1P (1992).